RAP CONFERENCE PROCEEDINGS, VOL. 8, PP. 1–4, 2023
ISSN 2737-9973 (ONLINE) | DOI: 10.37392/RAPPROC.2023.01
RAP-PROCEEDINGS.ORG

TOWARDS THE IMPLEMENTATION OF A PHANTOM FOR THE LOW CONTRAST EVALUATION OF ELECTRONIC PORTAL IMAGING DETECTORS (EPID): A THEORETICAL STUDY

Nektarios Kalyvas[1*], Marios K. Tzomakas[1], Vasiliki Peppa[2], Antigoni Alexiou[2], Georgios Karakatsanis[2], Anastasios Episkopakis[3,4], Christos Michail[1], Ioannis Valais[1], George Fountos[1], Ioannis S. Kandarakis[1]

[1]Radiation Physics, Materials Technology and Biomedical Imaging Laboratory, Department of Biomedical Engineering, University of West Attica, Egaleo, Athens, Greece
[2]General Hospital of Athens Alexandra, Department of Radiotherapy, Athens, Greece
[3]Elekta, Athens, Greece
[4]Medical Physics Laboratory, Medical School, National and Kapodistrian University of Athens, Athens, Greece

Abstract. *Electronic Portal Imaging Systems (EPIDs) are used in Radiotherapy treatment as part of the patient positioning verification check and for portal dosimetry purposes. The quality control of the imaging performance of an EPID is performed with dedicated phantoms. In this work, an examination through Monte Carlo (MC) simulation is presented in order to determine an appropriate step wedge phantom configuration for measuring low contrast differences in EPIDs. The PENELOPE based MC software package PenEasy was used. A simple geometry of a narrow cone beam with a cross section of 0.00053 cm² at 100 cm distance was assumed. A 2 MeV beam was considered to impinge on a 4 cm water equivalent phantom in conjunction with a metal sheet of Pb, Al, Fe or W positioned at 80 cm distance. At 100 cm distance a Gd2O2S:Tb scintillator, as part of an EPID responsible for detecting X-rays was assumed. The Gd2O2S:Tb thicknesses considered were 0.02cm and 0.03 cm. All the metal thicknesses were allowed to range from 0.1 cm to 1.5 cm per 0.1 cm step. The optical photons escaping to the Gd2O2S:Tb output were calculated by an analytical formula for each metal thickness. Hence, if a wedge metallic pattern from 0.1 cm to 1.5 cm is assumed to be constructed, then the optical photon output originating from each step, as well as the signal contrast between two steps would be known. It was found that a combination of Pb, Fe and W materials can be used for a step wedge phantom design.*

Keywords: *EPID, PenEasy, optical photon transport, low contrast, phantom*

1. INTRODUCTION

Electronic Portal Imaging Systems (EPIDs) are used in radiotherapy treatment as part of the patient positioning verification [1]-[3]. In recent years, the use of EPID systems for patient dosimetry purposes has also been reported [4]-[8]. It is therefore of essence to test the imaging performance of these detection devices. The assessment of the imaging performance of an EPID is performed with dedicated phantoms and methods as part of the quality control procedure [9], [10]. The phantoms may contain areas of low and high atomic number materials of different shapes so that parameters like image contrast, resolution and noise, to be evaluated [11], [12]. In this work the first step in the design of a phantom for image contrast assessment is presented. The phantom was assumed to follow a step wedge form inside a water equivalent material. The steps may allow for different contrast values calculation. Furthermore, by altering the material of the steps the achieved contrast may be diversified. The radiation interactions within the materials have been simulated by the PENELOPE based Monte Carlo (MC) simulation package [13]-[15]. The EPID was assumed to have a Gd_2O_2S:Tb based scintillator, also known as phosphor detector. The light generation in the Gd_2O_2S:Tb and its propagation towards the phosphor output was examined with analytical formulas obtained from literature [16]. It was found the Fe, W and Pb might be good choices for a step wedge phantom.

2. MATERIALS AND METHODS

2.1. X-ray photons interactions

The PENELOPE based MC software package PenEasy [17] was used in order to determine all X-ray photons energy deposition processes. A narrow monoenergetic 2 MeV photon beam of conical shape with a cross section equal to 0.00053 cm² at 100 cm distance was assumed. The beam was designed to impinge on a 4 cm water phantom, which was placed at 80 cm distance from the radiation source. At the output surface of the water phantom, opposite the beam entrance, different metal sheets of Pb, Al, Fe or W were considered. The metal thickness was allowed to range from 0.1 cm to 1.5 cm in 0.1 cm steps. A separated simulation was executed per each metal type and

* nkalyvas@uniwa.gr

thickness combination. At a distance of 100 cm from the X-ray source, corresponding to the isocenter of a LINAC, that is 20 cm beyond the water-metal combination, a Gd_2O_2S:Tb phosphor material was placed. The thicknesses of Gd_2O_2S:Tb considered were 0.02 cm and 0.03 cm. The simulation setup can be seen in Figure 1. The presented setup considers the EPID at the dosimetric calibration point of a LINAC, that is the isocenter.

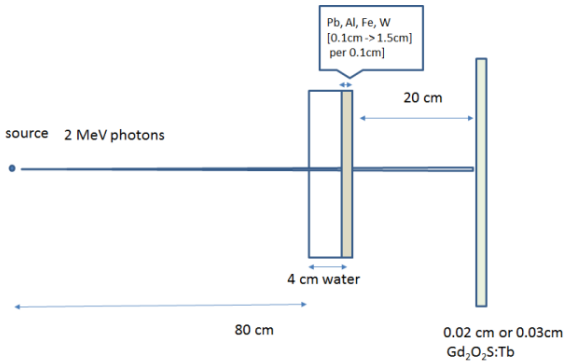

Figure 1. Graphical representation of the MC simulation geometry for testing the energy absorption in Gd_2O_2S:Tb for different metal sheets

2.2. Optical photons creation and propagation

Gd_2O_2S:Tb is utilized in EPID systems [2], [11], [12] since it efficiently absorbs the X-ray photons and converts the absorbed X-ray energy to optical photon energy. The optical photons that escape the phosphor part of the EPID are subsequently absorbed into the silicon pixelated array and finally converted to bit values. During this work it has been assumed that the number of optical photons escaping the scintillator can provide information regarding the signal, as well as for the signal differences i.e. the contrast. The creation of the optical photon energy per absorbed X-ray is described by the intrinsic conversion efficiency (n_C) describing the percentage of the absorbed X-ray power converted to optical photon power. If the absorbed X-ray energy (E) and the optical photon energy (E_λ) are known, then the calculation of $(E/E_\lambda)n_C$ is the number of the optical photons created in the scintillator [16], [18].

The number of the optical photons escaping the scintillator (L) can be described by a literature-based equation [18]:

$$L = \sum_i E_{abs} \frac{n_C}{E_\lambda} Q_i(E) M_i \qquad (1)$$

The reasoning behind Equation 1 is that the Gd_2O_2S:Tb thickness (T) can be divided into N layers of equal dimension Δt and the contribution of each layer i, i=1 to N, to the output can be summed. In Equation 1, E_{abs} is the energy from one photon absorbed in the scintillator, while $Q_i(E)$ is the contribution of layer i to the total absorbed energy fraction in the scintillator. Therefore the product of $E_{abs}Q_i(E)$ corresponds to the energy absorbed in layer i and the calculation of $(E_{abs}Q_i(E)/E_\lambda)n_C$ provides the number of the optical photons generated in layer I [18].

Only a fraction of these optical photons, denoted hereafter as M_i will escape to the output. M_i is a function of optical photon transport parameters in mass and can be calculated by the following formula [16]:

$$M_i = \frac{\tau\rho_1(\sigma+\tau\rho_0)e^{\sigma i\Delta t} + \tau\rho_1(\sigma-\tau\rho_0)e^{-\sigma i\Delta t}}{(\sigma+\tau\rho_0)(\sigma+\tau\rho_1)e^{\sigma T} - (\sigma-\tau\rho_0)(\sigma-\tau\rho_1)e^{-\sigma T}} \qquad (2)$$

where σ is the reciprocal diffusion length and τ is the inverse relaxation length, both functions of the optical photon absorption and scattering coefficients. Parameter ρ accounts for the optical photon reflection phenomena in the phosphor output (ρ_o) or input (ρ_i) [16]. Typical values for the calculation of the parameters of equations 1 and 2 were obtained from literature as: E_λ=2.46eV, n_C=0.18, σ=30 cm²/g [16], τ= σ /0.03 [16], [18]=1000 cm²/g and ρ_o, ρ_i were set equal to 1 [19].

2.3. Contrast calculation

The MC simulation was executed for different metal and thickness combinations. For each combination, a corresponding E_{abs} in Gd_2O_2S:Tb was calculated. The value of $Q_i(E)$ considered was the one calculated only for the water part of the phantom. Therefore, for each metal and its thickness, a unique E_{abs} was estimated by MC and the corresponding L value was subsequently derived by using equations 1 and 2. The differences of the L values are a measure of contrast for different metal sheets thicknesses, or steps. If the difference is calculated per 1 step (0.1 cm), per 2 steps (0.2 cm) etc., then the potential of step wedge shaped metallic structure placed at the exit of the water phantom can be considered to act as a contrast phantom.

In this work, the step contrast (SC) was calculated as:

$$SC = \frac{L_s - L_{s+step}}{L_s} \times 100\% \qquad (3)$$

where L_s is the signal value corresponding to the metal of thickness s and L_{s+step} is the signal corresponding to the metal of thickness $s+step$. The SC value corresponding of adjacent phantom steps provide the minimum perceived contrast for the specific material. The ability of the EPID to image the phantom signal differences may be associated with its ability to image real patient tissue differences, which in turn are associated with differences in the absorbed dose to the patient. Such a phantom may be useful to examine the extent of using an EPID device for patient dosimetry.

3. Results

The E_{abs} in Gd_2O_2S:Tb was calculated by MC simulation with an uncertainty below 1% for each metal type and thickness combination. When the Pb metal was considered the E_{abs} variations in Gd_2O_2S:Tb ranged from 7.7 keV to 4.9 keV and from 4.7 keV to 3 keV for scintillator thickness of 0.03 cm and 0.02 cm, respectively. The corresponding values for Al were approximately 10 keV and approximately 6.2 keV for all the Al metal thicknesses. The Fe metal sheets induced higher energy absorption in the scintillator when compared to that of Pb. Specifically, E_{abs} ranged from 5.5 keV to 4.9 keV and from 8.8 keV to 7.8 keV for Gd_2O_2S:Tb thickness of 0.02 cm and 0.03 cm, respectively. The corresponding values for W which were the lowest of all were calculated as 7.5 keV to 3.5 keV and from 4.5 keV to 2.1 keV, respectively.

In Figure 2, the Percentage Depth Dose (PDD) (i.e. $Q_i(E)$) of the fractional energy absorption distribution for different depth positions in Gd_2O_2S:Tb, as calculated by MC is demonstrated. The uncertainty of the simulation was below 1.5% for both 0.02 cm and 0.03 cm scintillator thicknesses. It may be observed from the figure that the peak dose is near the entrance of the phosphor material. The shape of the curve is sigmoid, although for the 0.03 cm thickness a linear absorption trend is demonstrated from 60 μm to 210 μm depths. This result differs when compared to the shape of PDD curves of water phantoms. The differences can be attributed to the highest atomic number and density of Gd_2O_2S:Tb with respect to water. Both the atomic number and density affect the probability of X-ray absorption and scatter. In addition, the sudden drop near the exit of the phosphor material might be due to the effect of the air after the material which alters the number of backscatter photons.

In Figure 3, the number of optical photons per X-ray, as it has been calculated by Equation 1 is shown. The higher values are observed for Al metal sheet, since its lower density of 2.7 g/cm³ compared to 11.35 g/cm³ of Pb, 19.3 g/cm³ of W and 7.87 g/cm³ of Fe [20] inhibits radiation absorption. Therefore more radiation impinge on Gd_2O_2S:Tb surface increasing light yield.

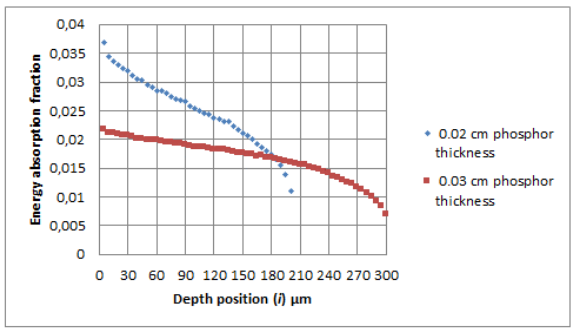

Figure 2. The fractional percent depth dose, $Q_i(E)$, as calculated by MC simulation for 0.02 cm and 0.03 cm Gd_2O_2S:Tb thicknesses

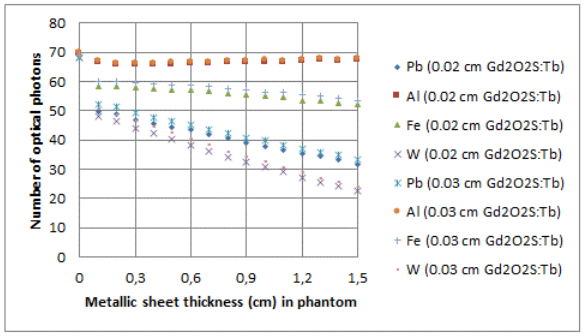

Figure 3. The number of optical photons escaping Gd_2O_2S:Tb for all metal types, metal sheet thickness and scintillator thickness combinations

In Figure 4, the contrast for Pb, Al, Fe and W for 0.02 cm Gd_2O_2S:Tb, as calculated by Equation 3 is shown. The thinner part L_s in Equation 3 is compared to a thicker part $L_{s+contrast\ step}$ for contrast steps 0.1 cm, 0.2 cm, 0.3 cm and 0.4 cm metal sheet.

It can be seen from Figure 4 that Al as a material cannot provide reliable signal differences, at least for the specific simulation geometry and energy deposition uncertainty. If Pb, Fe and W are considered, then contrast calculations ranging from 2% for Fe up to 20% for W can be safely obtained. These values are related to the signal value differences between the steps. On the contrary an almost unchanged value like the case of Al cannot contribute to reassuring signal differences as shown in Figure 4 and Figure 5. Similar, conclusions can be derived when the 0.03 cm phosphor thickness is considered. The corresponding contrast results are shown in Figure 5.

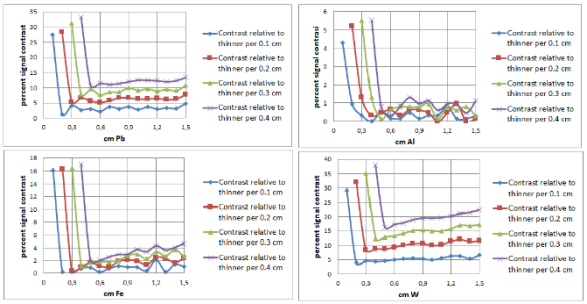

Figure 4. Optical photon percent signal contrast as calculated by Equation 3 relative to thinner part L_s for 0.02 cm Gd_2O_2S:Tb thickness

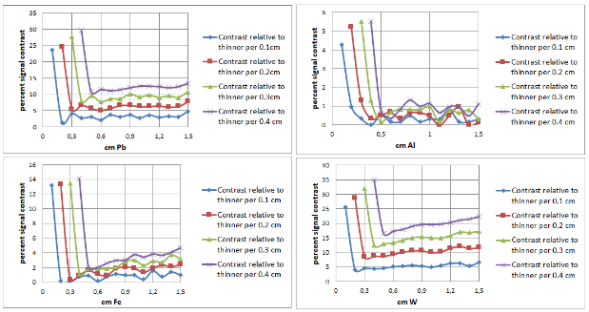

Figure 5. Optical photon percent signal contrast as calculated by Equation 3 relative to thinner part L_s for 0.03 cm Gd_2O_2S:Tb thickness

The presented results of Figure 3 are affected by the geometry of the simulation and specially by the distance between the X-ray source and the EPID [21]. In clinical LINAC setups the EPID is in a distance larger than 100 cm. This may affect the beam scatter component entering the scintillator and the E_{abs} values calculated. We do not however perceive this difference as an obstacle for proposing a phantom design.

Despite the aforementioned concerns the construction of a step wedge phantom with Pb, Fe and W seems a prominent solution for contrast evaluation. The contrast range would be specific for every LINAC, since it is affected by the operating MV as well as the presence or not of a flattening filter [22].

4. Conclusion

An initial theoretical study was performed to determine possible materials for fashioning a step wedge phantom for EPID quality control procedures. It was found that Pb, W and Fe could be utilized.

References

1. S. -H. Baek et al., "Clinical Efficacy of an Electronic Portal Imaging Device versus a Physical Phantom Tool for Patient-Specific Quality Assurance," *Life*, vol. 12, no. 11, 1923, Nov. 2022.
DOI: 10.3390/life12111923
PMid: 36431058
PMCid: PMC9694583
2. L. E. Antonuk, "Electronic portal imaging devices: a review and historical perspective of contemporary technologies and research," *Phys. Med. Biol.*, vol. 47, no. 6, pp. R31 – R65, Mar. 2002.
DOI: 10.1088/0031-9155/47/6/201
PMid: 11936185
3. C. K. McGarry, M. W. D. Grattan, V. P. Cosgrove, "Optimization of image quality and dose for Varian aS500 electronic portal imaging (EPIDs)," *Phys. Med. Biol.*, vol. 52, no. 23, pp. 6865 – 6877, Dec. 2007.
DOI: 10.1088/0031-9155/52/23/006
PMid: 18029980
4. A. Mans et al., "3D Dosimetric verification of volumetric-modulated arc therapy by portal dosimetry," *Radiother. Oncol.*, vol. 94, no. 2, pp. 181 – 187, Feb. 2010.
DOI: 10.1016/j.radonc.2009.12.020
PMid: 20089323
5. K. Ślosarek et al., "Portal dosimetry in radiotherapy repeatability evaluation," *J. Appl. Clin. Med. Phys.*, vol. 22, no. 1, pp. 156 – 164, Jan. 2021.
DOI: 10.1002/acm2.13123
PMid: 33314643
PMCid: PMC7856497
6. W. van Elmpt et al., "A literature review of electronic portal imaging for radiotherapy dosimetry," *Radiother. Oncol.*, vol. 88, no. 3, pp. 289 – 309, Sep. 2008.
DOI: 10.1016/j.radonc.2008.07.008
PMid: 18706727
7. L. C. G. G, Persoon et al., "Interfractional trend analysis of dose differences based on 2D transit portal dosimetry," *Phys. Med. Biol.*, vol. 57, no. 20, pp. 6445 – 6458, Oct. 2012.
DOI: 10.1088/0031-9155/57/20/6445
PMid: 23001452
8. I. Olaciregui-Ruiz, R. Rozendaal, B. Mijnheer, M. van Herk, A. Mans, "Automated in vivo portal dosimetry of all treatments," *Phys. Med. Biol.*, vol. 58, no. 22, pp. 8253 – 8264, Nov. 2013.
DOI: 10.1088/0031-9155/58/22/8253
PMid: 24201085
9. F. Cremers et al., "Performance of electronic portal imaging devices (EPIDs) used in radiotherapy: image quality and dose measurements," *Med. Phys.*, vol. 31, no. 5, pp. 985 – 996, May 2004.
DOI: 10.1118/1.1688212
PMid: 15191282
10. S. Y. Son et al., "Evaluation of image quality for various electronic portal imaging devices in radiation therapy," *J. Radiol. Sci. Technol.*, vol. 38, no. 4, pp. 451 – 461, Dec. 2015.
DOI: 10.17946/JRST.2015.38.4.16
11. B. K. Rout, M. C. Shekar, A. Kumar, K. K. D. Ramesh, "Quality control test for electronic portal imaging device using QC-3 phantom with PIPSpro," *Int. J. Cancer Ther. Oncol.*, vol. 2, no. 4, 02049, Sep. 2014.
DOI: 10.14319/ijcto.0204.9
12. I. J. Das et al., "A quality assurance phantom for electronic portal imaging devices," *J. Appl. Clin. Med. Phys.*, vol. 12, no. 2, pp. 391 – 403, Feb. 2011.
DOI: 10.1120/jacmp.v12i2.3350
PMid: 21587179
PMCid: PMC5718680
13. I. J. Das, F. Salvat, *PENELOPE: a Code system for Monte Carlo simulation of electron and photon transport*, OECD Nuclear Energy Agency, Issy-les-Moulineaux, France, 2015.
Retrieved from:
https://www.oecd-nea.org/upload/docs/application/pdf/2020-01/nsc-doc2015-3.pdf
Retrieved on: Jun. 12, 2023
14. J. Sempau, E. Acosta, J. Baro, J. M. Fernández-Varea, F. Salvat, "An algorithm for Monte Carlo simulation of coupled electron-photon transport," *Nucl. Instrum. Methods Phys. Res. B,* vol. 132, no. 3, pp. 377 – 390, Nov. 1997.
DOI: 10.1016/S0168-583X(97)00414-X
15. J. Baro, J. Sempau, J. M. Fernández-Varea, F. Salvat, "PENELOPE: An algorithm for Monte Carlo simulation of the penetration and energy loss of electrons and positrons in matter," *Nucl. Instrum. Methods Phys. Res. B*, vol. 100, no. 1, pp. 31 – 46, May 1995.
DOI: 10.1016/0168-583X(95)00349-5
16. C. M. Michail et al., "Experimental and theoretical evaluation of a high resolution CMOS based Detector under X-ray imaging conditions," *IEEE Trans. Nucl. Sci.*, vol. 58, no. 1, pp. 314 – 322, Feb. 2011.
DOI: 10.1109/TNS.2010.2094206
17. J. Sempau, A. Badal, L. Brualla, "A PENELOPE-based system for the automated Monte Carlo simulation of clinacs and voxelized geometries-application to far-from-axis fields," *Med. Phys.*, vol. 38, no. 11, pp. 5887 – 5895, Nov. 2011.
DOI: 10.1118/1.3643029
PMid: 22047353
18. I. Kandarakis, D. Cavouras, G. S. Panayiotakis, C. D. Nomicos, "Evaluating x-ray detectors for radiographic applications: a comparison of ZnSCdS:Ag with Gd2O2S:Tb and Y2O2S:Tb screens," *Phys. Med. Biol.*, vol. 42, no. 7, pp. 1351 – 1373, Jul. 1997.
DOI: 10.1088/0031-9155/42/7/009
PMid: 9253044
19. N. Kalyvas, P. Liaparinos, "Analytical and Monte Carlo comparisons on the optical transport mechanisms of powder phosphors," *Opt. Mater.*, vol. 88, pp. 396 – 405, Feb. 2019.
DOI: 10.1016/j.optmat.2018.12.006
20. *NIST Physical Measurement Laboratory Elemental Data Index: X-ray Form Factor, Attenuation and Scattering Tables*, NIST, Gaithersburg (MD), USA.
Retrieved from:
https://physics.nist.gov/PhysRefData/Elements/index.html
Retrieved on: Jun. 15, 2023
21. D. Parsons, J. L. Robar, "The effect of copper conversion plates on low Z target image quality," *Med. Phys.*, vol. 39, no. 9, pp. 5362 – 5371, Sep. 2012
DOI: 10.1118/1.4742052
PMid: 22957604
22. A. Kosunen, D. W. Rogers, "Beam quality specification for photon beam dosimetry," *Med. Phys.*, vol. 20, no. 4, pp. 1181 – 1188, Jul. 1993.
DOI: 10.1118/1.597150
PMid: 8413028